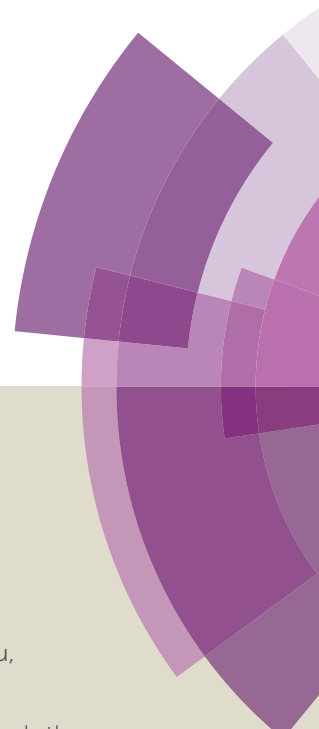


Journal of Materials Chemistry A

Accepted Manuscript



This article can be cited before page numbers have been issued, to do this please use: H. Song, Q. Zhu, X. Zheng and X. Chen, *J. Mater. Chem. A*, 2015, DOI: 10.1039/C5TA00280J.



This is an *Accepted Manuscript*, which has been through the Royal Society of Chemistry peer review process and has been accepted for publication.

Accepted Manuscripts are published online shortly after acceptance, before technical editing, formatting and proof reading. Using this free service, authors can make their results available to the community, in citable form, before we publish the edited article. We will replace this *Accepted Manuscript* with the edited and formatted *Advance Article* as soon as it is available.

You can find more information about *Accepted Manuscripts* in the [Information for Authors](#).

Please note that technical editing may introduce minor changes to the text and/or graphics, which may alter content. The journal's standard [Terms & Conditions](#) and the [Ethical guidelines](#) still apply. In no event shall the Royal Society of Chemistry be held responsible for any errors or omissions in this *Accepted Manuscript* or any consequences arising from the use of any information it contains.

Cite this: DOI: 10.1039/c0xx00000x

www.rsc.org/xxxxxx

ARTICLE TYPE

One-step synthesis of three-dimensional graphene/multiwalled carbon nanotubes/Pd composite hydrogel: an efficient recyclable catalyst for Suzuki coupling reactionsHui-qing Song ^a, Qian Zhu ^a, Xue-jing Zheng ^a, Xing-guo Chen ^{a, b, *}

⁵ Received (in XXX, XXX) Xth XXXXXXXXX 20XX, Accepted Xth XXXXXXXXX 20XX
DOI: 10.1039/b000000x

In this paper, a simple one-pot hydrothermal procedure to create three-dimensional (3D) graphene/multiwalled carbon nanotubes/Pd (G/MWCNTs/Pd) composite hydrogel with unique porous nanostructure was reported. During the formation of the G/MWCNTs/Pd composites, 2D graphene sheets and 1D MWCNTs were self-assembled to form interconnected porous microstructures and ultrafine Pd NPs were in situ grown on the 3D carbon-based skeleton simultaneously. In the as-obtained nanocomposites, MWCNTs not only prevented the close restacking of graphene sheets to increase the specific surface area but also provided an additional transport path to the catalyst surfaces which facilitated reactant transport. The G/MWCNTs/Pd composites proved to be an efficient, recyclable, and robust catalyst for the Suzuki cross-coupling reactions under mild aerobic conditions, which was attributed to the 3D macroporous framework with high specific surface area, numerous activation sites, and efficient transport pathways for improving the catalytic performance. Moreover, catalyst separation could be easily achieved by simple filtration, and the catalyst could be reused at least six runs without significant loss in catalytic activity. Additionally, nearly no Pd species was released from the G/MWCNTs/Pd composites during the catalytic reactions, showing the heterogeneity in the present catalysis system.

1. Introduction

It is well known that palladium (Pd)-catalyzed Suzuki cross-coupling transformations constitute a widely used method for the C–C bond formation in organic synthesis and industrial processes.^{1, 2} Currently the Suzuki cross-coupling reactions are performed mostly in homogeneous Pd catalytic systems in spite of the fact that it requires toxic and expensive phosphine ligands, which brings about unnecessary waste and hazard to the environment. Furthermore, further removal of Pd from the reaction systems is highly desirable due to the restriction of the catalysts in the industrial reuse. Therefore, from the viewpoint of green chemistry, heterogeneous catalysts centered around the use of Pd NPs are well-recognized because they have more advantages, such as the ease of work-up, the easy separation of products, and the recovery and regeneration of catalysts.¹⁻⁴ Unfortunately, Pd NPs without stabilization are prone to agglomerate due to their high surface area-to-volume ratio, which may lead to deactivation of catalysts.^{5, 6} A promising strategy to solve the issue could be the development of heterogeneous systems where active Pd species are immobilized on solid supports, which could maximize the active surface area of catalysts and improve their catalytic activity and durability during

the catalytic cycles. Among the various supports studied, the flexible graphene that provides much larger surface area for the dispersion of Pd NPs makes it quite promising for catalysis.

Graphene, a two-dimensional (2D) monolayer of sp²-hybridized carbon atoms patterned in a hexagonal lattice, with the advantages of large specific surface area, outstanding electrical conductivity, superior mechanical flexibility, and easy functionalization, have attracted widespread attention.^{7, 8} It is generally believed that the graphene-based catalysts not only raise the nanosized catalyst surface area for electron transport but also provide better mass transport of reactants to catalysts.⁹ However, in graphene-based composites, the graphene sheets easily form irreversible agglomerates driven by the strong Van der Waals interaction, which greatly compromises the superiority of the intrinsic high specific surface area of graphene.^{10, 11} Recently, three-dimensional (3D) carbon nanostructures made by connecting 2D planar graphene and 1D carbon nanotubes (CNTs) opened a new avenue for enhancing the surface area of materials.¹²⁻¹⁵ In the resulting 3D porous carbon nanostructures, the MWCNTs can efficiently inhibit the aggregations of the graphene sheets and maximize the surface area of 3D nanostructures for increasing the accessibility of the reactants to the catalyst surfaces.^{10, 16, 17} Besides, the 3D graphene/CNT

hybrids consist of abundance oxygen-containing functional groups, which can grip nanoparticles tight on the carbon framework and form a robust nanoarchitecture. Considerable effort has been devoted to fabricating the 3D graphene/CNT hybrids via various methods, including chemical vapor deposition,^{18, 19} microwave method,^{13, 14} atomic layer deposition,⁹ etc. However, some methods suffer from multistage synthesis processes, processing difficulties or expensive apparatus, etc. Recently, Wang et al.²⁰ reported the 3D Pd-CNT-GH composites via a self-assembled process, while the Pd NPs were about 30 nm in size. Generally, the intrinsic catalytic properties of metal NPs closely depend on their dimension, size and morphology.²¹ Hence, it is worthwhile to exploit a simple, low-cost, green, and scalable self-assembly method to form 3D carbon nanostructures with controlled NPs in size.

In this paper, we reported a facile one-step hydrothermal approach to prepare macroscopic graphene/multiwalled carbon nanotubes/Pd (G/MWCNTs/Pd) composite hydrogel with 3D interconnected networks under the self-assembly of GO sheets and MWCNTs, in which Pd NPs were in situ simultaneously grown on the 3D carbon framework. In this architecture, MWCNTs could bridge adjacent graphene sheets and restrain the aggregation of graphene sheets, resulting in a high contact area between the reactants and catalysts which could greatly improve the catalytic activity. The resulting 3D G/MWCNTs/Pd composites, when served as the catalyst for the Suzuki cross-coupling reactions, exhibited remarkable catalytic performances due to high porosity, high surface area, and robust chemical and mechanical stability. Additionally, the 3D G/MWCNTs/Pd composites showed wonderful cycling stability.

2. Experimental section

2.1. Materials

Graphite powder was purchased from Sigma-Aldrich. Raw multiwalled carbon nanotubes (MWCNTs) were supplied from Chengdu Organic Chemicals Co., Ltd. (Chengdu, China). Palladium chloride (PdCl_2 , >99%) was obtained from Sun Chemical Technology Co., Ltd. (Shanghai, China). Glucose was commercially available from Sinopharm Chemical Reagent Co., Ltd. (Shanghai, China). All the organic substrates were acquired from J&K Scientific Ltd. and Aladdin Reagent Co., Ltd. All other chemical reagents were used as received without further purification. Deionized water was used throughout the experiments.

2.2. Preparation of graphene oxide (GO)

GO was prepared by oxidation of natural graphite powder according to a modified Hummers method.⁷ Briefly, graphite powder (1 g) and NaNO_3 (0.5 g) were added to concentrated sulfuric acid (23 mL) under stirring in an ice bath. Under vigorous agitation, KMnO_4 (3.0 g) was slowly added into the cooled acid solution mixture maintaining temperature below 20 °C. Then, the ice bath was removed and the reaction system was stirred at 35 °C for about 30 min. Next, 46 mL of deionized water was added slowly, and the mixture was further stirred for 1 h with increasing the temperature to 98 °C. Finally, 140 mL of deionized water was added followed by a slow addition of 10 mL of H_2O_2 (30%), turning the color of the solution from dark-brown to

yellow. The as-obtained suspension was washed with 5% HCl and then deionized water by repeated centrifugation. Then the product was dialyzed through a dialysis membrane (retained molecular weight: 8-14 kDa) for a week to completely remove the residual salts and acids, and the suspensions were vacuum-dried at 65 °C to get GO sheets.

2.3 Preparation of 3D G/MWCNTs/Pd composite hydrogel

Before use, the raw MWCNTs (0.5 g) were chemically shortened and carboxylated by treat with concentrated HNO_3 (50 mL) at 60 °C under vigorous stirring for 12 h, producing carboxylic acid groups at the defect sites.²² Then the mixture was filtered and washed with deionized water, the obtained solid was employed as purified MWCNTs in the next steps.

The self-assembled 3D G/MWCNTs/Pd composites were synthesized via a facile one-step hydrothermal process. In a typical experiment, a 30 mL GO (1.5 mg mL^{-1}) aqueous dispersion was mixed with 15 mg MWCNTs (the mass ratio of GO to MWCNTs was 3:1) with the aid of ultrasonication for 2 h to form a homogeneous GO/MWCNTs suspension. Subsequently, 7.0 mg PdCl_2 was added to the above dispersion and sonicated for 0.5 h to achieve the electrostatic adsorption of Pd^{2+} ions on GO/MWCNTs, and the pH of the mixture was adjusted to about 9.0 with 1 mol/L NaOH aqueous solution. After that, 1.8 g glucose as reducing agent was added to form a stable homogeneous solution by sonication for 30 min, then the resulting mixture was sealed tightly in a Teflon-lined stainless steel autoclave and subjected to an elevated temperature of 120 °C in air oven for 24 h. After cooling to room temperature, the as-obtained black gel-like 3D cylinder was immersed in deionized water overnight to remove the residual ion and then freeze-dried into an aerogel for further use. For comparison, the MWCNTs/Pd without any additional GO and the 3D rGO/Pd hydrogel without any additional MWCNTs were fabricated using the similar procedures to that of G/MWCNTs/Pd. The Pd content was found to be 3.55 wt% for G/MWCNTs/Pd, 3.76 wt% for MWCNTs/Pd and 4.42 wt% for rGO/Pd by inductively coupled plasma atomic emission spectrometry (ICP-AES).

2.4. Characterization

Powder X-ray diffraction (XRD) patterns were performed on a D/MAX-2000 diffractometer (Rigaku, Japan) with Cu K α radiation ($\lambda = 1.54178 \text{ \AA}$). Raman spectra were obtained using a Dilor LABRAM-1B multichannel confocal microspectrometer with a 532 nm laser excitation. FT-IR spectra were recorded on a Nicolet Nexus 670 fourier transform infrared spectrometer (FT-IR, America) using KBr pellets. The microstructures of the samples were characterized by the field-emission scanning electron microscopy (FESEM, S-4800, Japan) and the transmission electron microscopy (TEM, Hitachi-600, Japan) with an energy dispersive X-ray analyzer (EDX). N_2 adsorption-desorption isotherms were acquired on a TriStar II 3020 analyzer (Micromeritics, USA). The specific surface areas (S_{BET}) were calculated using the Brunauer-Emmett-Teller (BET) model and the pore-size-distribution curves were obtained from the adsorption branches using the non-local density functional theory (NLDFT) method. X-ray photoelectron spectra (XPS) measurements were carried out on a PHI-5702 multifunctional spectrometer equipped with an Al K α exciting source. The Pd

content of the catalysts was measured by inductively coupled plasma atomic emission spectrometry (ICP-AES, Thermo Jarrel Ash, Franklin, MA, USA).

2.5. General procedure for the Suzuki coupling reactions

The Suzuki coupling reactions were carried out in a 25 mL three-neck flask under air atmosphere. In a typical experiment, aryl halide (1 mmol), phenylboronic acid (1.2 mmol), K_2CO_3 (2 mmol), catalyst (0.5 mol% of Pd) and EtOH/H₂O (v/v=1:1, 8 mL) were mixed and stirred at 60 °C for a specified time. The reaction progress was monitored by thin layer chromatography (TLC) at regular intervals. After the completion of the reaction, the catalyst was separated out by simple filtration and the filtrate was extracted with ethyl acetate, followed by analyzed by gas chromatography (GC, Varian 450) equipped with a capillary column (30 m, 0.25 mm i.d., CP-5) and an FID detector. N₂ was used as the carrier gas and the column temperature was maintained at 100 °C. The reaction yield was calculated through using n-dodecane as internal standard, which was reported as average value from at least three independent experiments.

For recycling, the catalyst was easily recovered by filtration and then washed thoroughly with diethylether, followed by deionized water and finally by dichloromethane, and then dried under vacuum at 40 °C for the next run.

2.6. Hot filtration test

The separated hot filtration test was conducted by carrying out the reaction of bromobenzene with phenylboronic acid under the optimized conditions. After 30 min, the reaction mixture was filtered at the reaction temperature in order to avoid possible precipitation of leached Pd species on the catalyst surface upon cooling. Then the reaction solution was further stirred for another 2 h at 60 °C, and the reaction progress was examined by GC analysis.

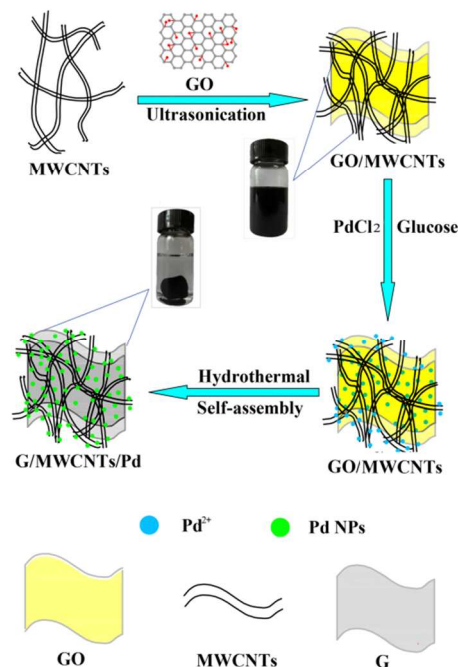
2.7. Solid-phase poisoning test

The solid-phase poisoning test was performed using iodobenzene and phenylboronic acid as coupling partners and adequate amount of poly(4-vinylpyridine) as a poisoning agent was introduced to the reaction under the optimized Suzuki conditions.

3. Results and discussion

A schematic illustration of the preparation process of the self-assembled 3D G/MWCNTs/Pd composite hydrogel was shown in Scheme 1, and the detailed experimental steps for the resulting composites were listed in the Experimental Section. Because of the abundant oxygen-containing functional groups, GO (Fig. S1a) and MWCNTs (Fig. S1b) could disperse well in water by sonication to produce a homogeneous suspension and MWCNTs are adsorbed onto the GO surface or inserted into the interspace of GO sheets, which is important for forming the uniform 3D structure.¹⁷ During the formation of composite hydrogels, several reactions could happen: firstly, the surface oxygen-containing functional groups and defects on GO and MWCNTs can act as nucleation sites and bind with Pd²⁺ ions by electrostatic force.^{23, 24} Then, the Pd²⁺ ions could be in situ reduced to Pd(0) NPs by glucose, which also increased the

mechanical strength of the self-assembled structure under the hydrothermal condition.²⁵ Meanwhile, an efficient self-assembly driven by the hydrophobic, electrostatic repulsion and the π - π interactions may occur and generated a 3D structure of composite hydrogel.



Scheme 1 Schematic illustration of the fabrication process of the 3D G/MWCNTs/Pd composite hydrogel.

In order to further investigate the crystal phase and structure information of the materials, the XRD patterns of the as-obtained GO, MWCNTs and the G/MWCNTs/Pd composites were shown in Fig. 1. The XRD pattern of GO showed a typical 2 θ diffraction peak at 9.9° indexed to the (002) crystal face with the d-spacing of 0.90 nm, which is much larger than the d-spacing (0.34 nm) of the pristine graphite (002) reflection. The expansion of the interlayer distance is attributed to the oxidation-induced expansion, due to the presence of oxygen-containing functional groups on the graphene sheets and some atomic scale structural defects.²⁶ And, the characteristic (002) diffraction peak of the MWCNTs was observed at 25.9°, which corresponds to an interlayer distance of 0.35 nm. The pattern of the G/MWCNTs/Pd composites exhibited a broad reflection at about 25.8° corresponding to the graphite-like structure (002) with the d-spacing (0.35 nm), which indicated that GO can be reduced during the hydrothermal conditions and was also a sign of a more disordered stacking and uniform dispersion of the graphene sheets in the as-prepared 3D framework.^{27, 28} Furthermore, the characteristic (002) peaks from MWCNTs and graphene sheets were overlapped, also suggesting the good graphitization of GO through the hydrothermal treatment. Besides this, the well-resolved peaks at 40.1°, 46.6°, 68.1° for the G/MWCNTs/Pd composites could be assigned to the (111), (200) and (220) lattice planes of a face-centered cubic (fcc) Pd crystalline structure (JCPDS no. 05-0681), and no new phase was detected in the

G/MWCNTs/Pd composites. And the average crystallite size of Pd calculated using the Debye-Scherrer equation is about 7.9 nm, slightly larger than the TEM-determined size. In addition, the XRD patterns of rGO/Pd and MWCNTs/Pd (Fig. S2) were investigated and they revealed the indicative diffraction peaks of Pd crystals, indicating the Pd NPs were well anchored on the rGO and MWCNTs, respectively.

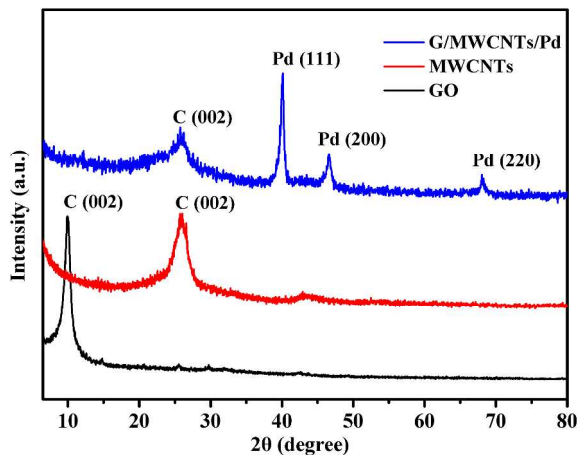


Fig. 1 XRD patterns of as-prepared GO, MWCNTs and the G/MWCNTs/Pd composites.

Raman spectroscopy, a powerful tool in studying structural changes of carbonaceous materials, was employed to gain information about the vibrational properties of GO, MWCNTs and the G/MWCNTs/Pd composites. As shown in Fig. 2a, two prominent characteristic peaks at around 1355 and 1590 cm^{-1} were presented in the Raman spectra, which can be ascribed to the D and G peaks of the carbon materials, respectively. The G band is assigned to the E_{2g} vibrational mode of sp^2 carbon atoms patterned in hexagonal lattice corresponding to ordered sp^2 bonded carbon, whereas the D band is attributed to structural defects in the crooked graphene sheet and the disorder carbon.²⁹ As known, the intensity ratio of the D band to the G band (I_D/I_G) in the Raman spectrum is used as an indicator of the disorder degree and the average size of the sp^2 domains in graphitic materials.²⁷ It is found that the value of I_D/I_G of in the 3D G/MWCNTs/Pd composites was 1.24, which increased markedly when compared with those of GO (0.92) and MWCNTs (0.99), indicating the improvement of the disordered levels. The more disordered carbon structure in the G/MWCNTs/Pd composites could be explained that the removal of oxygen-containing functional groups led to a decrease in the average size of the in-plane sp^2 domains after the hydrothermal treatment.²⁸

The FT-IR spectra of GO and the prepared G/MWCNTs/Pd composites in the region of 4000–500 cm^{-1} were shown in Fig. 2b. In the IR spectrum of GO, the absorption peaks at 3430, 1728, 1621, 1384, 1224 and 1067 cm^{-1} were observed, which can be indexed to the stretching vibrations of O–H, C=O in carboxyl group, C=C in aromatic ring, C–OH, carboxy C–O and epoxy C–O stretching vibrations, respectively.^{12, 30, 31} However, the oxygen functional group peaks at 1728, 1384 and 1067 cm^{-1} were almost disappeared in the spectrum of the G/MWCNTs/Pd composites, indicating the effective reduction of GO to the reduced graphene oxide by glucose during the hydrothermal

process. The result was in accordance with that of Raman spectroscopy analysis. In addition, it is also found that the bands of GO at 1621 cm^{-1} ascribed to the skeletal vibrations of unoxidized graphitic domains red-shifted to 1574 cm^{-1} after the hydrothermal reduction, which may be due to the addition of multiwalled carbon nanotubes and improvement of the conjugation degree of graphene and MWCNTs.¹⁶

Then the elemental compositions and the chemical state of Pd particles in the G/MWCNTs/Pd composites were investigated by X-ray photoelectron spectroscopy (XPS). From the survey scan spectra in Fig. 3a, it can be seen that the G/MWCNTs/Pd composites displayed a distinct Pd signal compared with the XPS spectrum of GO/MWCNTs, as expected. In the high-resolution Pd 3d XPS spectrum (see Fig. 3b), the binding energy of the doublet peak at 335.7 eV (assigned to Pd 3d_{5/2}) and 341.0 eV (assigned to Pd 3d_{3/2}) can be attributed to the Pd (0) state.³² Furthermore, no peaks corresponding to Pd²⁺ in the XPS spectrum were observed, which indicated that Pd²⁺ ions have been reduced to Pd NPs by glucose during the hydrothermal process.²⁵ In the C1s spectrum of GO/MWCNTs (Fig. 3c), four pronounced deconvoluted binding energy peaks were identified as sp^2 carbon at 284.6 eV, C–O at 286.6 eV, C=O at 288.2 eV and O–C=O at 289.7 eV.^{9, 33} Compared with GO/MWCNTs, most oxygen-containing functional groups were reduced by glucose in the formation process of the G/MWCNTs/Pd composite hydrogel, which was verified by the increasing intensity of sp^2 C–C bonds at 284.6 eV and the decreasing intensity of the oxygen-containing carbon (C–O at 286.6 eV, carbonyl C=O at 288.2 eV and carboxyl O–C=O at 289.7 eV),³⁴ as shown from the deconvoluted C1s spectra of the as-prepared G/MWCNTs/Pd composites in Fig. 3d. In agree with XRD and Raman spectra measurements, they all indicated that the G/MWCNTs/Pd composites presented effective reducing not only for oxygen-containing functional groups but also for the decorated Pd NPs.

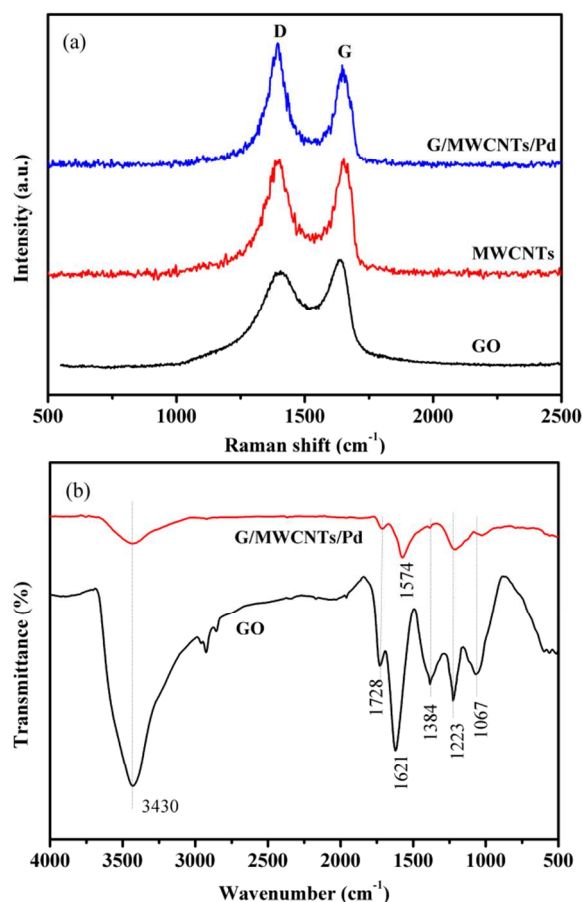


Fig. 2 (a) Raman spectra of GO, MWCNTs and the G/MWCNTs/Pd composites and (b) FT-IR spectra of GO and the G/MWCNTs/Pd composites.

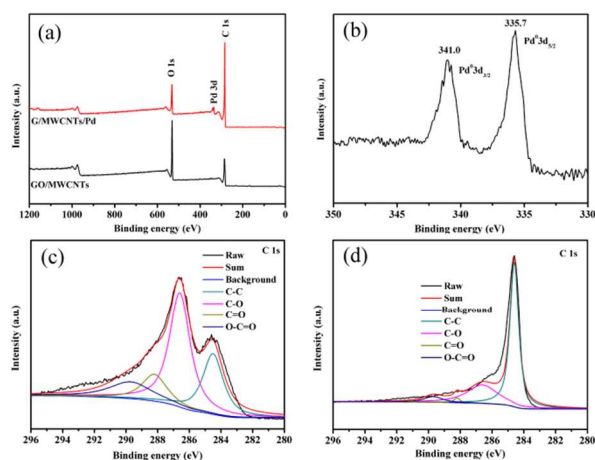


Fig. 3 XPS spectra of GO/MWCNTs and the G/MWCNTs/Pd composites: (a) survey scan, (b) Pd 3d spectrum of the G/MWCNTs/Pd composites, (c) C 1s spectrum of GO/MWCNTs and (d) C 1s spectrum of the G/MWCNTs/Pd composites.

The morphology and structure of the self-assembled 3D G/MWCNTs/Pd nanostructures were characterized by means of scanning electron microscopy (SEM) and transmission electron microscopy (TEM). Fig. 4a and b showed the corresponding SEM images of the as-prepared G/MWCNTs/Pd composite hydrogel, revealing a well-defined and interconnected 3D grapheme-based network microstructure with continuous

macropores ranging from submicrometer to several micrometers. From Fig. 4a and b, it also showed that MWCNTs were well distributed on the surface of graphene sheets as well as inserted into the graphene sheets, which acted as bridges to effectively prevent graphene sheets from restacking and enlarged the spaces among sheets, leading to a loose architecture.³⁵ Compared with G/MWCNTs/Pd, rGO/Pd (Fig. S3a) displayed a similar porous structure, whereas MWCNTs/Pd (Fig. S3b) consisted of randomly orientated and entangled MWCNTs with Pd NPs anchored on them. The detailed structure of the G/MWCNTs/Pd composites was further examined by TEM measurements. As presented in Fig. 4c, Pd NPs were uniformly attached on the graphene surface and multiwalled carbon nanotubes, and the average diameter was about 4.5–6.0 nm (Fig. S4a). The image shown in Fig. 4c also presented that the MWCNTs were dispersed on the graphene surface and/or inserted into the interspace of the graphene sheets to form a 3D structure framework, validating the introduction of MWCNTs onto the graphene sheets.^{9, 35} According to the previous reports,^{10, 36, 37} the interaction between metallic NPs with graphene layers can enhance their interface contact and suppress the dissolution and agglomeration of NPs, thereby promoting the chemical activity and stability of the composites. The lattice spacing of the Pd NPs detected in the high-resolution TEM (HRTEM) image (Fig. 4d) was calculated to be 0.22 and 0.19 nm, which is in accordance with the (111) and (200) planes of Pd crystals, respectively.³⁸ The EDX analysis in Fig. S5 showed that the G/MWCNTs/Pd composites consisted of C, O, and Pd elements, indicating the successful fabrication Pd NPs on the carbon skeleton. For comparison, we also presented the TEM images of the rGO/Pd and MWCNTs/Pd composites (Fig. S3c–f). TEM and HRTEM images of rGO/Pd and MWCNTs/Pd revealed the crystalline Pd NPs with the size of 4.5–6.5 nm (Fig. S4b and c) were well anchored on the graphene layers and MWCNTs, respectively.

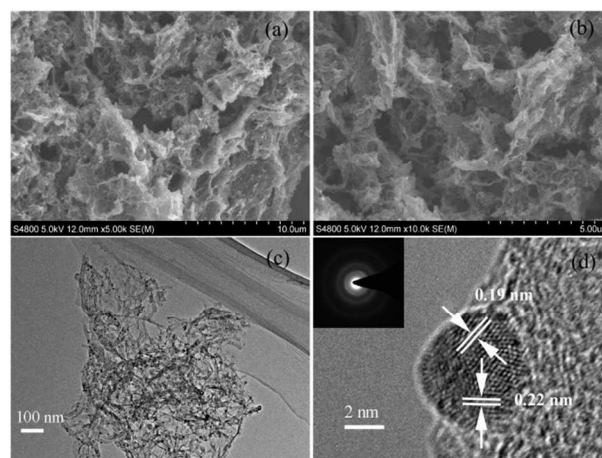


Fig. 4 SEM images of the G/MWCNTs/Pd composites (a and b). Representative TEM (c) and HRTEM (d) images of the G/MWCNTs/Pd composites. Inset shows the corresponding SAED pattern.

The Brunauer–Emmett–Teller (BET) specific surface area and porous structure of the G/MWCNTs/Pd composites were further investigated by nitrogen adsorption-desorption analysis, with typical isotherms shown in Fig. 5. It can be seen that the G/MWCNTs/Pd composites featured the type IV isotherms with an H3-type hysteresis loop ($P/P_0 = 0.45–1.0$), confirming the

presence of mesoporous and macroporous structures in the composites.¹⁹ Based on the above results, we think that the G/MWCNTs/Pd composites is porous, which is consistent with the microstructure observed by the SEM images. As a comparison, those of the rGO/Pd and MWCNTs/Pd composites have also been provided, and they exhibited the typical type IV isotherms, indicating the porosity of the samples.³¹ The BET surface areas and pore volume of the G/MWCNTs/Pd composites were measured to be 142.3 m² g⁻¹ and 0.52 cm³ g⁻¹, which are evidently superior to that of rGO/Pd (87.8 m² g⁻¹ and 0.35 cm³ g⁻¹) and MWCNTs/Pd (77.3 m² g⁻¹ and 0.31 cm³ g⁻¹), respectively. It turned out that MWCNTs can effectively prevent the aggregation of graphene sheets to increase the specific surface area of the G/MWCNTs/Pd composites after the introduction of MWCNTs.^{17, 35} The pore size distributions of the composites obtained on basis of the non-local density functional theory (NLDFT) method also deliver a consistent picture in the pore size viewpoint. As shown in Fig. 5b-d, the G/MWCNTs/Pd and rGO/Pd composites displayed the pores in the range of 3-100 nm and most of the pores in MWCNTs/Pd lay in 10-100 nm range, which is associated with different porous architectures resulting from the different building blocks.³¹ Combining the results with SEM measurements, the larger specific surface area and the unique hierarchical porous feature of the G/MWCNTs/Pd composites would provide efficient transport pathways to the interior cavities, thus leading to better catalytic performance.

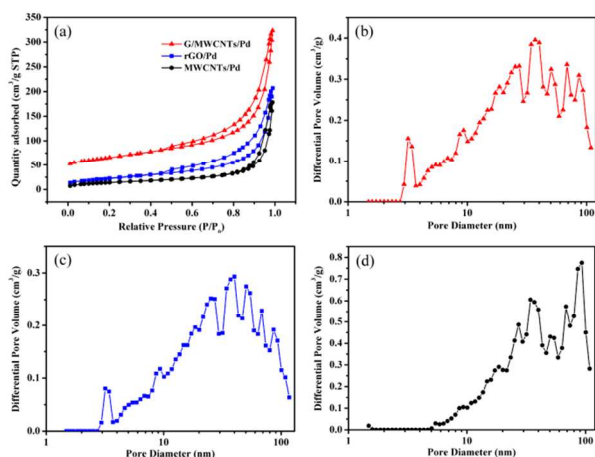


Fig. 5 N₂ adsorption/desorption isotherms (a) and pore size distribution of G/MWCNTs/Pd (b), rGO/Pd (c) and MWCNTs/Pd (d).

Catalytic performance

To evaluate the catalytic activity of the as-prepared 3D G/MWCNTs/Pd composites, Suzuki coupling reaction one of the representative Pd-catalyzed reactions was carried out as a model reaction. It is worth pointing out that base and solvent can remarkably influence the reactivity of the Suzuki coupling reaction. Here, we chose iodobenzene and phenylboronic acid as the model substrates to optimize the reaction conditions under aerobic condition. As showed in Table 1, poor yields were obtained when the model reaction was performed in polar aprotic solvents, such as CH₃CN, THF, acetone and DMF (Table 1, entries 1-3 and 5). In contrast, the relatively high yields were achieved with the use of polar protic solvents, such as MeOH and EtOH (Table 1, entries 6 and 7). Interestingly, when H₂O was

adopted as the solvent, the reaction was sluggish (Table 1, entries 4); however, the addition of H₂O to DMF or EtOH led to a profound increase in activity. Notably high activity of the catalyst G/MWCNTs/Pd can be achieved by using the mixed solvent DMF/H₂O (v/v=1:1) and EtOH/H₂O (v/v=1:1) (Table 1, entries 8 and 9), due to the good solubility of organic substrates and inorganic base in co-solvents. The mixed solvent endowed the base with good solubility in water for activating arylboronic acid, resulting in a higher reactivity in aqueous medium. And the result was consistent with previous work on solvent effects in the Suzuki reaction.³⁹ Among the solvents screened, EtOH/H₂O (v/v=1:1) was the preferred solvent for the cross-coupling reaction with the highest yield of >99% (Table 1, entry 9). Next, various bases, such as Cs₂CO₃, Na₂CO₃, KOH, Na₃PO₄·12H₂O, NaAc and Et₃N, were investigated for the coupling reaction under the same conditions. And, the results indicated that inorganic bases were more effective than organic bases like NaAc and Et₃N (Table 1, entries 14 and 15), probably due to two factors: (1) partial inhomogeneity of organic bases in aqueous phase and (2) inorganic bases were more effective in activate arylboronic acid towards the formation of a boronate complex which can facilitate the subsequent transmetalation process to enhance the reactive activity as compared to organic bases in the reaction system. Among the tested bases, it seemed that K₂CO₃ and Cs₂CO₃ were preferred for the reaction system (Table 1, entries 9 and 10), because they accomplished activation of the palladium better than other bases.⁴⁰ Finally, K₂CO₃ was chosen as the base for the coupling reaction because of its economic material benefit. As demonstrated above, the Suzuki coupling reactions were carried out at 60 °C in air using K₂CO₃ as base and EtOH/H₂O (v/v=1:1) as reaction medium.

Table 1 Optimization of the reaction conditions for Suzuki cross-coupling reaction of iodobenzene with phenylboronic acid catalyzed by G/MWCNTs/Pd^a

Entry	Solvent ^c	Base	Time (min)	Yield ^b (%)
1	CH ₃ CN* (35.94)	K ₂ CO ₃	20	25
2	THF* (7.58)	K ₂ CO ₃	20	20
3	Acetone* (20.70)	K ₂ CO ₃	20	23
4	H ₂ O* (78.36)	K ₂ CO ₃	20	44
5	DMF* (36.31)	K ₂ CO ₃	20	34
6	MeOH* (32.66)	K ₂ CO ₃	20	72
7	EtOH* (24.55)	K ₂ CO ₃	20	86
8	DMF/ H ₂ O	K ₂ CO ₃	20	98
9	EtOH/H ₂ O	K ₂ CO ₃	15	>99
10	EtOH/H ₂ O	Cs ₂ CO ₃	15	>99
11	EtOH/H ₂ O	Na ₂ CO ₃	15	91
12	EtOH/H ₂ O	KOH	15	83
13	EtOH/H ₂ O	Na ₃ PO ₄ ·12H ₂ O	15	68
14	EtOH/H ₂ O	NaAc	15	35
15	EtOH/H ₂ O	Et ₃ N	15	56

^a Reaction conditions: iodobenzene (1 mmol), phenylboronic acid (1.2 mmol), base (2 mmol), catalyst (0.5 mol%), solvent (8 mL, for mixed solvent, the volume ratio is 1:1) at 60 °C under air.

^b GC yields. ^c the dielectric constant under 25 °C.

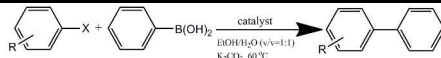
* represents the polar aprotic solvent

☆ represents the polar protic solvent

With the optimal reaction conditions in hand, the scope of the G/MWCNTs/Pd-catalyzed Suzuki reactions was examined by

coupling various substituted aryl halides with phenylboronic acid, and the results were summarized in Table 2. The data presented in Table 2 showed that aryl iodides and aryl bromides were converted effectively to the corresponding coupling products with good yields. Aryl iodides bearing an electron-donating or an electron-withdrawing group exhibited high reactivity and afforded satisfactory yields within 15–30 min (Table 2, entries 1–7). Fortunately, the catalyst G/MWCNTs/Pd also exhibited excellent catalytic activity for aryl bromides with substituents such as $-\text{CH}_3$, $-\text{NO}_2$, $-\text{CN}$, $-\text{OCH}_3$, $-\text{OH}$ and $-\text{NH}_2$ corresponding to respective biaryl products with high yields (Table 2, entries 8–15). Further studies indicated that the less active chlorobenzene and its derivatives coupled with phenylboronic acid needed a longer time to obtain a moderate yield (Table 2, entries 16–18). It is well-known that substituents in the aryl halides have an effect on the Suzuki cross-coupling reactions. In agreement with previous studies,^{41, 42} aryl halides with electron-withdrawing substituents gave higher yields than that of electron-donating ones. However, aryl iodides containing the $-\text{COOH}$ group proceeded less efficiently than other electron-withdrawing substituents, which may be attributed to the decrease in basicity of the reaction medium.⁴¹ It is noteworthy that 2-iodophenol with $-\text{OH}$ group and 2-bromonitrobenzene with $-\text{NO}_2$ group, which are sterically hindered, offered good yields but not as excellent as their *para*-substituted aryl halides (Table 2, entries 4, 5, 10, 11). The result revealed that the *para*-substituted aryl halides showed better reactivity than *ortho*-substituted aryl halides. As a contrast, the catalytic performances of an equal amount of rGO/Pd and MWCNTs/Pd for the Suzuki coupling reaction were also studied (Table 2). From these results, it is found that G/MWCNTs/Pd exhibited a more pronounced catalytic activity for the Suzuki coupling reaction than the rGO/Pd and MWCNTs/Pd catalyst under the optimal reaction conditions. In view of the three composites, the enhanced catalytic performance of G/MWCNTs/Pd can be attributed to the effect of porous structure on the effective access of the substrates to the exposed active sites with fast diffusion, which was closely related to its higher BET surface area.

Table 2 Scope of the Suzuki cross-coupling reaction catalyzed by 40 different supported Pd-based catalysts under optimized conditions^a



Entry	R	X	Time (h)	Yield ^b (%)		
				G/MWCNTs /Pd	rGO/Pd	MWCNTs/Pd
1	H	I	1/4	>99	76	64
2	4-COCH ₃	I	1/4	96	81	68
3	4-NH ₂	I	1/4	91	68	55
4	2-OH	I	1/4	86	64	46
5	4-OH	I	1/4	92	71	54
6	4-NO ₂	I	1/5	97	80	71
7	4-COOH	I	1/2	91	73	60
8	H	Br	1	95	78	69
9	4-CN	Br	1	96	83	73
10	4-NO ₂	Br	1	98	84	76
11	2-NO ₂	Br	1.5	89	69	62
12	4-CH ₃	Br	1.5	90	71	65
13	4-OCH ₃	Br	1.5	92	75	65
14	4-OH	Br	2	88	67	59
15	4-NH ₂	Br	2	94	73	63
16	H	Cl	6	46	14	9
17	4-OCH ₃	Cl	6	33	8	6
18	4-NO ₂	Cl	6	62	19	13

^a Reaction conditions: iodobenzene (1 mmol), phenylboronic acid (1.2 mmol), K₂CO₃ (2 mmol), catalyst (0.5 mol%), EtOH/H₂O (v/v=1:1, 8 mL) at 60 °C under air.

^b GC yields.

Recycling of the catalyst

Recycling is one of the most attractive advantages of the heterogeneous catalyst for practical applications, here we chose phenylboronic acid and iodobenzene as model substrates to test the reusability and lifetime of the G/MWCNTs/Pd catalyst under the optimized conditions mentioned above. As illustrated in Table 3, the catalyst was reused directly up to six consecutive cycles and remained the excellent catalytic efficiency without loss of catalytic selectivity and activity. The excellent recyclability of the catalyst could be attributed to the strong interaction between Pd NPs and oxygen-containing functional groups arising from carbon-based material.⁴³ The TEM measurement of the recovered G/MWCNTs/Pd catalyst (after 6 runs) indicated that Pd NPs were still well dispersed without obvious aggregation (Fig. S6), which further confirmed the high catalytic activity and good stability of the catalyst. Another key factor to be investigated is the stability of the catalyst. To examine the stability of the G/MWCNTs/Pd catalyst, the Suzuki coupling reaction of iodobenzene and phenylboronic acid was repeated using the as-prepared catalyst for three months. As shown in Fig. S7, the catalyst exhibited similarly high catalytic activity in three months, suggesting that the G/MWCNTs/Pd catalyst was very stable which was not air-sensitive and can be used within three months without obvious loss of activity.

Hot filtration and leaching test

Metal leaching of the catalyst is of critical importance and in order to test if Pd species was leaching out from the catalyst during reaction, a hot-filtration test was performed by coupling bromobenzene with phenylboronic acid. When the reaction was stirred for 30 min (71% yield, GC), the solid catalyst was removed and the residual activity of the mother liquor was

studied. Moreover, no significant change in either the bromobenzene conversion or the cross-coupled biphenyl was observed in the filtrate. And, ICP-AES analysis of the filtrate confirmed the absence of Pd species in the liquid phase. Subsequently, the catalyst after six cycles was further analyzed by ICP-AES. The results showed that the Pd content in the G/MWCNTs/Pd composites after six runs was 3.46 wt% and the Pd content in the fresh catalyst was 3.55 wt%. And the amount of the leached Pd collected after six cycles in the reaction mixture was 20 ppb, the smaller amount of Pd leaching suggested the strong affinity between Pd NPs with carbon skeleton which effectively prevented the Pd active sites from leaching. The results demonstrated that the effect of trace amounts of Pd leaching on the present catalyst system can be neglected and the carbon support bound Pd NPs were responsible for the catalytic activity.

Table 3 Reusability of the G/MWCNTs/Pd catalyst for the Suzuki cross-coupling reaction of iodobenzene with phenylboronic acid

Runs	1	2	3	4	5	6
Yield	>99	99	97	96	97	94

Solid-phase poisoning test

To ascertain the heterogeneous nature of the catalyst used in our system, the solid-phase poisoning test was performed. Up to now, various poisons have been used to hinder the catalytic activity of homogeneous versus heterogeneous catalysts. In the study, we employed poly(4-vinylpyridine) as an effective Pd scavenger that could selectively coordinate and trap the homogeneous Pd species.⁴⁴ If Pd leached out during the aryl-coupling reaction, then poly(4-vinylpyridine) provided binding

sites for the leached Pd to form a complex and deactivated the active Pd species, thereby reduced the yield of the product. However, it is noted that the yield did not apparently change, indicating the Suzuki coupling reactions in the experiment were performed via a heterogeneous catalytic way. We could deduce that the catalyst was heterogeneous in nature and no significant leaching of Pd occurred during the coupling reaction.

In order to evaluate the efficiency of the G/MWCNTs/Pd catalyst, we compared the results obtained in this work with those reported elsewhere of recoverable Pd-based efficient heterogeneous catalysts.^{3, 38, 45-53} Taking iodobenzene reacting with phenylboronic acid as an example, the results were listed in Table 4. It can be seen that the present catalyst exhibited a better catalytic effect with the highest apparent turnover frequencies (TOF) of 799 h⁻¹ in comparison to other reported ones (Table 4, entry 12). Although some of them also obtained high yields, some toxic solvents (such as CH₂Cl₂, DMF, or DME) were used or longer reaction time or relatively high temperature was needed. These chemicals were less favorable than the ethanol used in this study. The G/MWCNTs/Pd catalyst seemed to be the best candidate, showing an excellent efficiency for the Suzuki cross-coupling reactions in terms of yield, cost, reaction time, selectivity, and reusability. Furthermore, we also compared the catalytic activities of G/MWCNTs/Pd with different supported Pd catalysts for the Suzuki cross-coupling reaction of aryl halide with phenylboronic acid,⁵⁴⁻⁵⁷ and the reactions were carried out at 60 °C in air using K₂CO₃ as base and EtOH/H₂O (v/v=1:1) as reaction medium. As demonstrated in Table S1, the catalyst G/MWCNTs/Pd exhibited the better catalytic activity.

Table 4 Catalytic performances of different Pd-based catalysts in the coupling of iodobenzene and phenylboronic acid

Entry	Catalyst	Solvent	Base	Temp (°C)	Time (h)	Yield (%)	TOF ^a (h ⁻¹)	Ref.
1	Pd/MFC	EtOH	K ₂ CO ₃	reflux	1	100	324.6	3
2	Pd NPs	H ₂ O	Na ₂ CO ₃	80	24	97.1	40.5	38
3	Pd-Fe ₃ O ₄	DME/H ₂ O=3:1	Na ₂ CO ₃	reflux	24	99	41.3	45
4	Pd@Mag-MSN	CH ₂ Cl ₂	K ₂ CO ₃	80	6	85	14.2	46
5	Pd/CNT-SiC	EtOH/H ₂ O=4:1	K ₃ PO ₄	60	1	98	350	47
6	Pd@CNPCs	DMF/H ₂ O=1:1	K ₂ CO ₃	50	1.5	96.7	644.6	48
7	MUA-Pd	DMF	NaOH	90	8	>99	6.2	49
8	Pd-CNT-ED-OH	DMF	Na ₂ CO ₃	110	24	94	13.1	50
9	Pd(0)/MCoS-1	H ₂ O	K ₂ CO ₃	70	5	98	98	51
10	Pd/NiFe ₂ O ₄	DMF/H ₂ O=1:1	Na ₂ CO ₃	90	1/12	97	196	52
11	sugar-derived PdNPs	iPrOH	K ₂ CO ₃	100	20	88	4.4	53
12	G/MWCNTs/Pd	EtOH/H ₂ O=1:1	K ₂ CO ₃	60	1/4	>99	799	this work

^a The apparent TOF value was measured as moles of product with per mole of Pd catalyst per hour.

4. Conclusions

In summary, the 3D G/MWCNTs/Pd composite hydrogel was fabricated successfully via a facile one-pot self-assembled approach, accompanied by an in situ growth process, where ultrafine Pd NPs were well-dispersed on the surface of the 3D carbon skeleton. The 3D G/MWCNTs/Pd composites endowed macroporous structure, large surface area and good durability, resulting in excellent catalytic activity and selectivity toward the Suzuki cross-coupling reaction with high yields. More significantly, the catalyst could be recovered easily and reused at least six runs without significant loss of the activity. Due to its

easy separation, recycling, air-stability, low cost and without the use of phosphine ligands, the 3D G/MWCNTs/Pd catalyst was highly desirable to address the environmental concerns. On the basis of the results, the 3D G/MWCNTs/Pd composite materials may promise huge potential for applications in industrial catalysis.

Acknowledgements

The authors are grateful for financial support from the National Natural Science Foundation of China (No. 21375053) and Special Doctorial Program Fund from the Ministry of Education of China (No. 20130211110039).

Notes and references

^a State Key Laboratory of Applied Organic Chemistry, College of Chemistry and Chemical Engineering, Lanzhou University, Lanzhou, Gansu 730000, China

^b Key Laboratory of Nonferrous Metal Chemistry and Resources Utilization of Gansu Province, Lanzhou University, Lanzhou, Gansu 730000, China

* Corresponding author

Xingguo Chen: Tel: 86-931-8912763, Fax: 86-931-8912582, E-mail:

chenxg@lzu.edu.cn

Electronic Supplementary Information (ESI) available: [details of any supplementary information available should be included here]. See DOI: 10.1039/b000000x/

1. A. Balanta, C. Godard and C. Claver, *Chem. Soc. Rev.*, 2011, 40, 4973.
2. L. X. Yin and J. Liebscher, *Chem. Rev.*, 2007, 107, 133.
3. M. Y. Zhu and G. W. Diao, *J. Phys. Chem. C*, 2011, 115, 24743.
4. P. W. Liu, Z. M. Dong, Z. B. Ye, W. J. Wang and B. G. Li, *J. Mater. Chem. A*, 2013, 1, 15469.
5. M. B. Thathagar, J. E. ten Elshof and G. Rothenberg, *Angew. Chem., Int. Ed.*, 2006, 45, 2886.
6. R. S. Underhill and G. J. Liu, *Chem. Mater.*, 2000, 12, 3633.
7. L. J. Cote, F. Kim and J. X. Huang, *J. Am. Chem. Soc.*, 2009, 131, 1043.
8. D. C. Marcano, D. V. Kosynkin, J. M. Berlin, A. Sinitskii, Z. Z. Sun, A. Slesarev, L. B. Alemany, W. Lu and J. M. Tour, *ACS Nano*, 2010, 4, 4806.
9. C. T. Hsieh, Y. Y. Liu, D. Y. Tzou and W. Y. Chen, *J. Phys. Chem. C*, 2012, 116, 26735.
10. H. Wang, H. Yi, X. Chen and X. Wang, *J. Mater. Chem. A*, 2014, 2, 1165.
11. J. H. Lee, N. Park, B. G. Kim, D. S. Jung, K. Im, J. Hur and J. W. Choi, *ACS Nano*, 2013, 7, 9366.
12. R. J. Chen, T. Zhao, J. Lu, F. Wu, L. Li, J. Z. Chen, G. Q. Tan, Y. S. Ye and K. Amine, *Nano Lett.*, 2013, 13, 4642.
13. S. H. Bae, K. Karthikeyan, Y. S. Lee and I. K. Oh, *Carbon*, 2013, 64, 527.
14. S. Vadahanambi, S. H. Lee, W. J. Kim and I. K. Oh, *Environ. Sci. Technol.*, 2013, 47, 10510.
15. R. T. Lv, T. X. Cui, M. S. Jun, Q. Zhang, A. Y. Cao, D. S. Su, Z. J. Zhang, S. H. Yoon, J. Miyawaki, I. Mochida and F. Y. Kang, *Adv. Funct. Mater.*, 2011, 21, 999.
16. M. Q. Sun, G. C. Wang, X. W. Li and C. Z. Li, *J. Power Sources*, 2014, 245, 436.
17. F. Y. Zeng, Y. F. Kuang, N. S. Zhang, Z. Y. Huang, Y. Pan, Z. H. Hou, H. H. Zhou, C. L. Yan and O. G. Schmidt, *J. Power Sources*, 2014, 247, 396.
18. X. C. Dong, H. Xu, X. W. Wang, Y. X. Huang, M. B. Chan-Park, H. Zhang, L. H. Wang, W. Huang and P. Chen, *ACS Nano*, 2012, 6, 3206.
19. H. Jiang, Y. H. Dai, Y. J. Hu, W. N. Chen and C. Z. Li, *ACS Sustainable Chem. Eng.*, 2014, 2, 70.
20. Z. Y. Zhang, T. Sun, C. Chen, F. Xiao, Z. Gong and S. Wang, *ACS Appl. Mater. Interfaces*, 2014, 6, 21035.
21. G. T. Fu, W. Han, L. F. Yao, J. Lin, S. H. Wei, Y. Chen, Y. W. Tang, Y. M. Zhou, T. H. Lu and X. H. Xia, *J. Mater. Chem.*, 2012, 22, 17604.
22. M. Eguilaz, R. Villalonga, P. Yanez-Sedeno and J. M. Pingarron, *Anal. Chem.*, 2011, 83, 7807.
23. G. Goncalves, P. A. A. P. Marques, C. M. Granadeiro, H. I. S. Nogueira, M. K. Singh and J. Gracio, *Chem. Mater.*, 2009, 21, 4796.
24. J. J. Yuan, J. W. Zhu, H. P. Bi, X. Q. Meng, S. M. Liang, L. L. Zhang and X. Wang, *Phys. Chem. Chem. Phys.*, 2013, 15, 12940.
25. Z. H. Tang, S. L. Shen, J. Zhuang and X. Wang, *Angew. Chem.*, 2010, 122, 4707.
26. C. T. Hsieh, J. S. Lin, Y. F. Chen, C. Y. Lin and W. Y. Li, *Mater. Chem. Phys.*, 2014, 143, 853.
27. J. Xu, S. L. Gai, F. He, N. Niu, P. Gao, Y. J. Chen and P. P. Yang, *J. Mater. Chem. A*, 2014, 2, 1022.
28. X. A. Chen, X. H. Chen, F. Q. Zhang, Z. Yang and S. M. Huang, *J. Power Sources*, 2013, 243, 555.
29. Y. W. Ma, L. Y. Sun, W. Huang, L. R. Zhang, J. Zhao, Q. L. Fan and W. Huang, *J. Phys. Chem. C*, 2011, 115, 24592.
30. S. Y. Yin, Y. Y. Zhang, J. H. Kong, C. J. Zou, C. M. Li, X. H. Lu, J. Ma, F. Y. C. Boey and X. D. Chen, *ACS Nano*, 2011, 5, 3831.
31. M. Kotal and A. K. Bhowmick, *J. Phys. Chem. C*, 2013, 117, 25865.
32. R. Li, P. Zhang, Y. M. Huang, P. Zhang, H. Zhong and Q. W. Chen, *J. Mater. Chem.*, 2012, 22, 22750.
33. T. Sun, Z. Y. Zhang, J. W. Xiao, C. Chen, F. Xiao, S. Wang and Y. Q. Liu, *Sci. Rep.*, 2013, 3, 2527.
34. H. P. Cong, X. C. Ren, P. Wang and S. H. Yu, *ACS Nano*, 2012, 6, 2693.
35. L. F. Shen, X. G. Zhang, H. S. Li, C. Z. Yuan and G. Z. Cao, *J. Phys. Chem. Lett.*, 2011, 2, 3096.
36. Z. S. Wu, S. B. Yang, Y. Sun, K. Parvez, X. L. Feng and K. Muellen, *J. Am. Chem. Soc.*, 2012, 134, 9082.
37. M. Yuan, A. P. Liu, M. Zhao, W. J. Dong, T. Y. Zhao, J. J. Wang and W. H. Tang, *Sens. Actuators, B-Chem.*, 2014, 190, 707.
38. A. Q. Zhang, M. Liu, M. Liu, Y. H. Xiao, Z. X. Li, J. L. Chen, Y. Sun, J. H. Zhao, S. M. Fang, D. Z. Jia and F. Li, *J. Mater. Chem. A*, 2014, 2, 1369.
39. Q. Xiao, S. Sarina, E. Jaatinen, J. F. Jia, D. P. Arnold, H. W. Liu and H. Y. Zhu, *Green Chem.*, 2014, 16, 4272.
40. L. Artok and H. Bulut, *Tetrahedron Lett.*, 2004, 45, 3881.
41. D. Saha, R. Sen, T. Maity and S. Koner, *Langmuir*, 2013, 29, 3140.
42. L. J. Zhang, Z. X. Su, F. L. Jiang, Y. F. Zhou, W. T. Xu and M. C. Hong, *Tetrahedron*, 2013, 69, 9237.
43. F. R. Chen, M. M. Huang and Y. Q. Li, *Ind. Eng. Chem. Res.*, 2014, 53, 8339.
44. J. M. Richardson and C. W. Jones, *Adv. Synth. Catal.*, 2006, 348, 1207.
45. Y. Jang, J. Chung, S. Kim, S. W. Jun, B. H. Kim, D. W. Lee, B. M. Kim and T. Hyeon, *Phys. Chem. Chem. Phys.*, 2011, 13, 2512.
46. S. Shylesh, L. Wang, S. Demeshko and W. R. Thiel, *Chemcatchem*, 2010, 2, 1543.
47. H. Yuan, H. Y. Liu, B. S. Zhang, L. Y. Zhang, H. H. Wang and D. S. Su, *Phys. Chem. Chem. Phys.*, 2014, 16, 11178.
48. P. Zhang, Z. H. Weng, J. Guo and C. C. Wang, *Chem. Mater.*, 2011, 23, 5243.
49. M. Cargnello, N. L. Wieder, P. Canton, T. Montini, G. Giambastiani, A. Benedetti, R. J. Gorte and P. Fornasiero, *Chem. Mater.*, 2011, 23, 3961.
50. E. Kim, H. S. Jeong and B. M. Kim, *Catal. Commun.*, 2014, 46, 71.
51. A. S. Roy, J. Mondal, B. Banerjee, P. Mondal, A. Bhaumik and S. M. Islam, *Appl. Catal., A*, 2014, 469, 320.
52. S. R. Borhade and S. B. Waghmode, *Beilstein J. Org. Chem.*, 2011, 7, 310.
53. J. E. Camp, J. J. Dunsford, E. P. Cannons, W. J. Restorick, A. Gadzhieva, M. W. Fay and R. J. Smith, *ACS Sustainable Chem. Eng.*, 2014, 2, 500.
54. S. K. Movahed, R. Esmatpoursalmani and A. Bazgir, *RSC Adv.*, 2014, 4, 14586.
55. S. K. Movahed, M. Dabiri and A. Bazgir, *Appl. Catal., A*, 2014, 488, 265.
56. Q. Zhang, H. Su, J. Luo and Y. Y. Wei, *Catal. Sci. Technol.*, 2013, 3, 235.
57. R. F. Nie, J. J. Shi, W. C. Du and Z. Y. Hou, *Appl. Catal., A*, 2014, 473, 1.